Langerhans cell (LC) proliferation mediates neonatal development, homeostasis, and inflammation–associated expansion of the epidermal LC network

Laurent Chorro,[1,2] Aurélien Sarde,[1] Mei Li,[3] Kevin J. Woollard,[1]
Pierre Chambon,[3] Bernard Malissen,[4] Adrien Kissenpfennig,[4]
Jean-Baptiste Barbaroux,[5] Richard Groves,[5] and Frédéric Geissmann[1,2]

[1]Centre for Molecular and Cellular Biology of Inflammation, Division of Immunobiology, Infection, and Inflammatory Diseases, King's College London, London SE1 1UL, England, UK
[2]Institut National de la Santé et de la Recherche Médicale (INSERM) U838, Universite Paris-Descartes, 75015 Paris, France
[3]Department of Functional Genomics, Institut de Génétique et de Biologie Moléculaire et Cellulaire, Centre National de la Recherche Scientifique (CNRS)/INSERM/Université de Strasbourg, 67404 Illkirch, France
[4]Centre d'Immunologie de Marseille-Luminy, INSERM U631, CNRS UMR6102, Université de la Méditerranée, Case 906, 13288 Marseille, Cedex 9, France
[5]St. John's Institute of Dermatology, Guy's Hospital, King's College London, London SE1 9RT, England, UK

The Journal of Experimental Medicine

Most tissues develop from stem cells and precursors that undergo differentiation as their proliferative potential decreases. Mature differentiated cells rarely proliferate and are replaced at the end of their life by new cells derived from precursors. Langerhans cells (LCs) of the epidermis, although of myeloid origin, were shown to renew in tissues independently from the bone marrow, suggesting the existence of a dermal or epidermal progenitor. We investigated the mechanisms involved in LC development and homeostasis. We observed that a single wave of LC precursors was recruited in the epidermis of mice around embryonic day 18 and acquired a dendritic morphology, major histocompatibility complex II, CD11c, and langerin expression immediately after birth. Langerin+ cells then undergo a massive burst of proliferation between postnatal day 2 (P2) and P7, expanding their numbers by 10–20–fold. After the first week of life, we observed low–level proliferation of langerin+ cells within the epidermis. However, in a mouse model of atopic dermatitis (AD), a keratinocyte signal triggered increased epidermal LC proliferation. Similar findings were observed in epidermis from human patients with AD. Therefore, proliferation of differentiated resident cells represents an alternative pathway for development in the newborn, homeostasis, and expansion in adults of selected myeloid cell populations such as LCs. This mechanism may be relevant in locations where leukocyte trafficking is limited.

CORRESPONDENCE
Frederic Geissmann:
frederic.geissmann@kcl.ac.uk

Abbreviations used: AD, atopic dermatitis; CDP, common DC precursor; GVHD, graft–versus–host disease; LC, Langerhans cell; MDP, macrophage DC precursor; PI, propidium iodide; TSLP, thymic stromal lymphopoietin; VDR, vitamin D receptor.

Current data indicate that many macrophage subsets and most DCs in nonlymphoid tissues and in the secondary lymphoid organs of mice originate and are renewed from bone-marrow hematopoietic stem cell–derived progenitors with myeloid-restricted differentiation potential (Fogg et al., 2006; Liu et al., 2009). However, exceptions must exist to this major pathway of macrophage and DC generation, because Langerhans cells (LCs) and microglia remain of host origin

after syngeneic bone marrow transplant (Merad et al., 2002; Ajami et al., 2007; Mildner et al., 2007), and LCs remain of donor origin after a limb graft (Kanitakis et al., 2004). Epidermal LCs have been shown to be a cycling population (Giacometti and Montagna, 1967; Czernielewski et al., 1985; Czernielewski and Demarchez, 1987). LC precursors were proposed to reside in the dermis (Larregina et al., 2001)

A. Kissenpfennig's present address is Centre for Infection and Immunity, School of Medicine, Dentistry, and Biomedical Sciences, Queen's University of Belfast, Belfast BT9 7BL, Northern Ireland, UK.

or in the hair follicle (Gilliam et al., 1998), and cells with features of proliferating LC precursors have been found in fetal and newborn skin (Elbe et al., 1989; Chang-Rodriguez et al., 2005). On the other hand, monocytes can give rise to LC-like cells in vitro (Geissmann et al., 1998; Mohamadzadeh et al., 2001), and LCs can be replaced by bone marrow–derived cells in a selected experimental setting, i.e., after allogeneic bone marrow transplant, UV light irradiation, and conditional genetic ablation (Katz et al., 1979; Frelinger and Frelinger, 1980; Merad et al., 2002; Bennett et al., 2005). The nature of the endogenous LC precursor is thus unclear.

LC development is controlled by M-CSF receptor and TGF-β1 (Borkowski et al., 1996; Ginhoux et al., 2006; Kaplan et al., 2007), but the LC precursor is particularly enigmatic because, in contrast to most organs, migration of leukocytes into the epidermis, as well as the brain, is rarely observed in a steady state; when such migration is observed, it is typically associated with inflammation. The mechanisms by which LCs develop and are renewed may differ from those involved in organs where hematopoietic cells circulate constantly, such as the spleen, liver, or lung. Although the roles of epidermal LCs remain controversial, recent evidence indicates a role as scavengers for viruses such as HIV-1 (de Witte et al., 2007) and possibly for carcinogens (Strid et al., 2008), as well as their role in promoting and regulating T cell–mediated immune responses (Bennett et al., 2007; Stoitzner et al., 2008; Elentner et al., 2009; Vesely et al., 2009). Understanding the mechanisms that control the development and homeostasis of DCs and macrophages in the skin or brain is thus of importance in understanding the pathophysiology of inflammation in these organs. In this study, we investigated the development of the LC network of the epidermis, and how it is maintained in a steady state and during epidermal inflammation.

RESULTS

CD115$^+$ FLT3$^-$ CD45$^+$ CX$_3$CR1$^+$ myeloid precursors colonize the epidermis between embryonic day 14 (E14) and E18 and differentiate into langerin$^+$ MHCII$^+$ CX$_3$CR1$^-$ LCs

Langerin$^+$ MHCII$^+$ cells become detectable in the epidermis after birth (Tripp et al., 2004); however, CD45$^+$ CD3$^-$ cells, putative LC precursors, are first found in the skin of E17 fetuses (Elbe et al., 1989). This LC precursor may be related to monocyte/macrophage and DC precursors, characterized by the expression of the chemokine receptor CX$_3$CR1 (Auffray et al., 2009) and the hematopoietic-restricted phosphatase CD45. Therefore, we investigated whether it was possible to track LC precursors in the skin by examining whole-mount stainings of skin and epidermal sheets from CX$_3$CR1-GFP reporter mice (Auffray et al., 2007). NK cells and epidermal γδ T cells can express CD11b and CX$_3$CR1, and are a source of false positives in the analysis of myeloid cells using CX$_3$CR1-GFP reporter mice; therefore, we used Rag$^{-/-}$ γc$^{-/-}$ CX$_3$CR1-GFP reporter mice devoid of lymphoid precursors and mature lymphocytes (Auffray et al., 2007).

We have previously shown that LCs develop normally in Rag$^{-/-}$ γc$^{-/-}$ mice, indicating that LC development is independent of the T cell lineage (Asli et al., 2004).

CX$_3$CR1-GFP$^+$ cells were already detectable in skin from E14 embryos but were located in the dermis and not in the epidermis (Fig. 1 A). CX$_3$CR1-GFP$^+$ cells were first observed in the epidermis, in between epithelial cells, at E18 (Fig. 1 A). Flow cytometry analysis indicated that E18 epidermal CX$_3$CR1-GFP cells expressed the M-CSF receptor (CD115, CSF-1R), the CD11b integrin Mac-1 (Fig. 1 B), and CD45 (Fig. 2 A), but did not express significant levels of the Ly6C antigen. E18 epidermal CX$_3$CR1-GFP cells lacked expression of Kit (CD117), FLT3 (CD135), CD11c, MHCII, and langerin, which characterize macrophage DC precursors (MDPs), common DC precursors (CDPs), preclassical DCs, and LCs (Fig. 1, B and C; and Fig. 2 A; Merad et al., 2008; Liu et al., 2009).

Between days 0 and 2 after birth, these epidermal CX$_3$CR1-GFP cells start to acquire a dendritic morphology and expression of langerin, MHCII, and CD11c, characteristics of differentiated LCs (Fig. 1 A and Fig. 2, A–D). At day 4 after birth, most CX$_3$CR1-GFP cells coexpressed langerin and MHCII (Fig. 2, D and E), indicating that at this stage, new CX$_3$CR1-GFP langerin$^-$ precursors are not recruited in the epidermis. Expression of CX$_3$CR1-GFP was then progressively lost by epidermal LCs (Fig. 2 E), and adult LCs do not express CX$_3$CR1 (Fig. 1 B). We did not observe any CX$_3$CR1-GFP cells in the epidermis of adult Rag$^{-/-}$ γc$^{-/-}$ CX$_3$CR1-GFP mice (Fig. 1 B and Fig. 2 E).

These data indicate that a single wave of myeloid CD45$^+$ CD115$^+$ CD11b$^+$ CX$_3$CR1-GFP$^+$ precursors is recruited in the epidermis before birth, around day E18, and differentiate into LCs in situ. These precursors have a phenotype distinct from the CDPs or preclassical DCs (Liu et al., 2007; Waskow et al., 2008). Their developmental relationship with bone marrow–derived cells that arise after E15 (Wolber et al., 2002; Bertrand et al., 2005) or with earlier E14 dermal CX$_3$CR1-GFP$^+$ cells, which are likely to derive from the fetal liver or yolk sac, remains to be investigated.

CD45$^+$ CX$_3$CR1$^+$ epidermal precursors were evenly distributed in the epidermis and did not cluster around hair follicles (Fig. 1 A). This is unlike the distribution observed in langerin–diphtheria toxin receptor mice after depletion, when bone marrow–derived cells were observed to colonize the epidermis in clusters (Bennett et al., 2005; Kaplan et al., 2007; Poulin et al., 2007).

Langerin$^+$ MHCII$^+$ cells proliferate massively and migrate to establish the LC network between postnatal day 4 (P4) and P7

From E18 to P2, the number of CD45$^+$ CX$_3$CR1$^+$ precursors remains low in the epidermis, at 50–100 cells/mm^2 (Fig. 3 A). However, between days 2 and 7, the number of newly differentiated LCs rapidly increased to reach 1,000/mm^2 (Fig. 3 A), whereas the size of individual LCs dramatically decreased, as estimated using intravital microscopy in
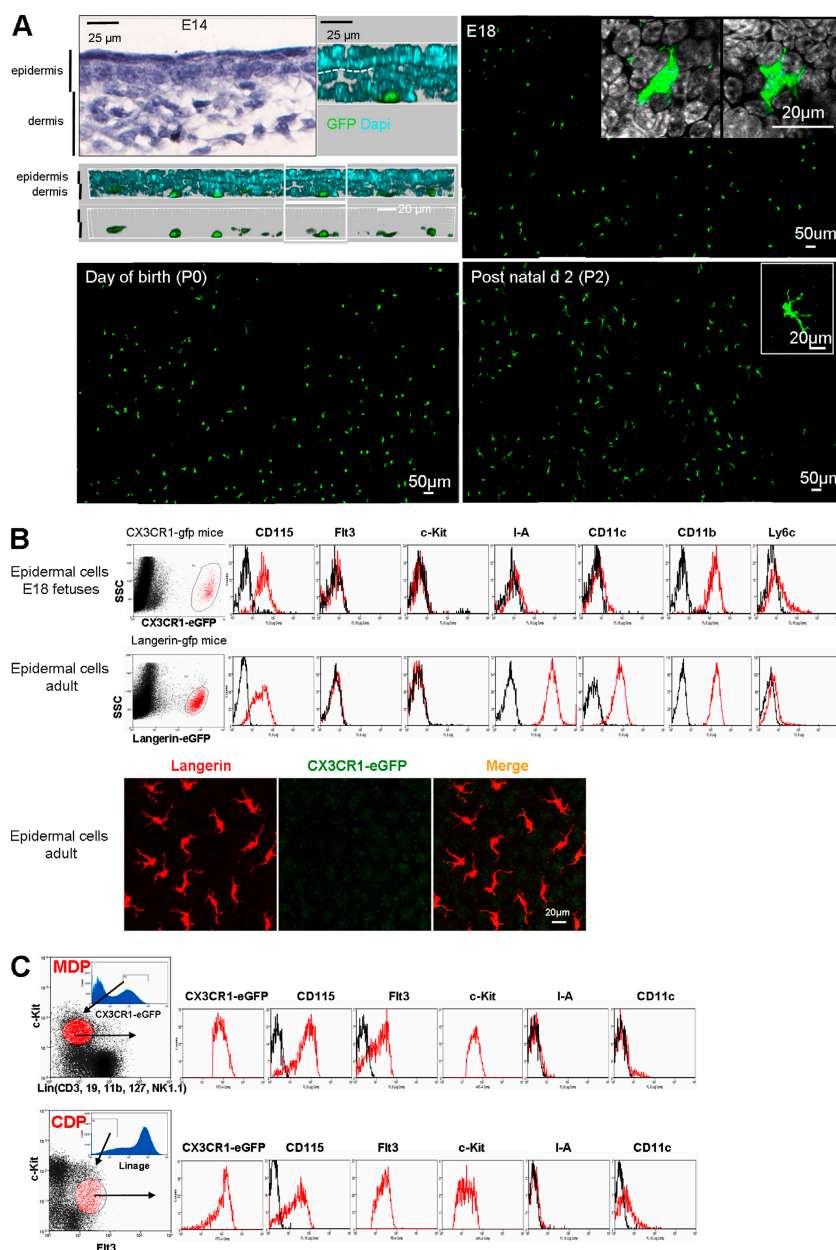
Figure 1. Early recruitment of a CX_3CR1^+ $CD45^+$ $CD115^+$ $CD11b^+$ myeloid precursor in the epidermis between E14 and E18. (A, top left) H&E staining and three-dimensional reconstruction of skin from E14 CX_3CR1-GFP $Rag^{-/-}$ $\gamma c^{-/-}$ mice. CX_3CR1^+ cells are labeled in green and nuclei are labeled in blue. Confocal Z-stacks were acquired using a Leica SP5 microscope. Images show a 2–4-μm thick virtual section of the tissue. The dashed line indicates the separation between the dermis and epidermis. CX_3CR1^+ cells can be detected in the dermis but not in the epidermis. Results are representative of 10 skin samples per mouse ($n = 4$). (top right and bottom) Tiled micrographs of epidermal sheets of CX_3CR1-GFP $Rag^{-/-}$ $\gamma c^{-/-}$ E18 fetuses and pups at P0 (the day of birth) and P2. CX_3CR1^+ cells are labeled in green. Tiles were obtained by assembling a series of maximal intensity projections of Z-stacks. (insets) Enlarged CX_3CR1^+ cells (green) and nuclei (white). CX_3CR1-expressing cells are first detected in the epidermis at E18, and acquire a dendritic shape between P0 and P2 ($n = 3–4$ mice for each time point). (B, top) Flow cytometry analysis of epidermal cells from E18 CX_3CR1-GFP $Rag^{-/-}$ $\gamma c^{-/-}$ embryos and 10-wk-old langerin-GFP mice. Cells were labeled with antibodies against CSF-1R (CD115), Flt3 (CD135), c-kit (CD117), I-A, CD11c, CD11b, and Lyc6 and analyzed by multicolor flow cytometry. Dot plots show the gate used for analysis of GFP-expressing LC precursors and adult LCs. Overlaid histograms show the expression of surface markers on gated GFP^+ cells (red line) and control (fluorescence minus one; black line). Results are representative of three to five experiments with similar results. (bottom) Micrographs display maximal intensity projections of Z-stacks from epidermal sheets of 10-wk-old CX_3CR1-GFP $Rag^{-/-}$ $\gamma c^{-/-}$ mice. CX_3CR1-expressing cells are labeled in green and langerin is labeled in red. Results are representative of 12 0.03-mm^2 Z-stacks per mouse ($n = 4$). Adult LCs do not express CX_3CR1 (GFP). (C) Flow cytometry analysis of bone marrow MDPs and CDPs. Bone marrow cells from adult CX_3CR1-GFP $Rag2^{-/-}$ $\gamma c^{-/-}$ mice were labeled with antibodies against lineage markers (CD11b, NK1.1, CD3, Ter119, and CD19), c-kit (CD117), Flt3 (CD135), CSF-1R (CD115), CD11c, and I-A and analyzed by multicolor flow cytometry. MDPs are defined as CX_3CR1^{high} (GFP) c-kit$^+$ lineage$^-$, whereas CDPs are defined as lineage$^-$ c-kit^{low} Flt3$^+$. Overlaid histograms show expression of surface markers on gated MDPs and CDPs (red line) over control (black line). Results are representative of three to five experiments with similar results. SSC, side scatter.

langerin-GFP reporter mice ([Fig. S1](#); Elbe et al., 1989; Kissenpfennig et al., 2005). Similar kinetics of LC expansion were observed in CCR2$^{-/-}$ mice (Fig. 3 A). The absence of epidermal CX$_3$CR1$^+$ langerin$^-$ cells at day 4 (Fig. 2 B) and the results from CCR2$^{-/-}$ mice indicated that LC expansion may rely on a mechanism distinct from the CCR2-dependent recruitment of precursors from blood that has been observed for the recruitment of LCs after UV treatment or genetic depletion (Ginhoux et al., 2006; Poulin et al., 2007).

Analysis of cell proliferation using Ki67 staining on epidermal sheets from Rag$^{-/-}$ γc$^{-/-}$ CX$_3$CR1-GFP and langerin-GFP mice indicated that 20% of myeloid CD45$^+$ CX$_3$CR1$^+$ LC precursors, scattered across the epidermis, expressed Ki67$^+$

at E18, whereas this number decreased to <10% at P0 and P2 (Fig. 3 B). No mitotic figures were observed in epidermal CX$_3$CR1$^+$ cells at P2 and P0, and in only 1 out of 800 cells was the presence of two nuclei in the same cytoplasm observed in the epidermis of an E18 embryo ([Fig. S2](#)). These data suggest that CX$_3$CR1$^+$ cells are derived from a proliferating precursor, whereas they do not actively proliferate inside the epidermis.

In contrast, analysis at day 4 after birth indicated that 60–70% of epidermal langerin$^+$ cells were recently cycling (Fig. 3 C). Three-dimensional reconstruction analysis of whole-mount epidermis identified numerous langerin$^+$ cells at various stages of the mitotic process (Fig. 3 D, [Fig. S3](#), and [Video 1](#)). To confirm in situ proliferation of LCs in the
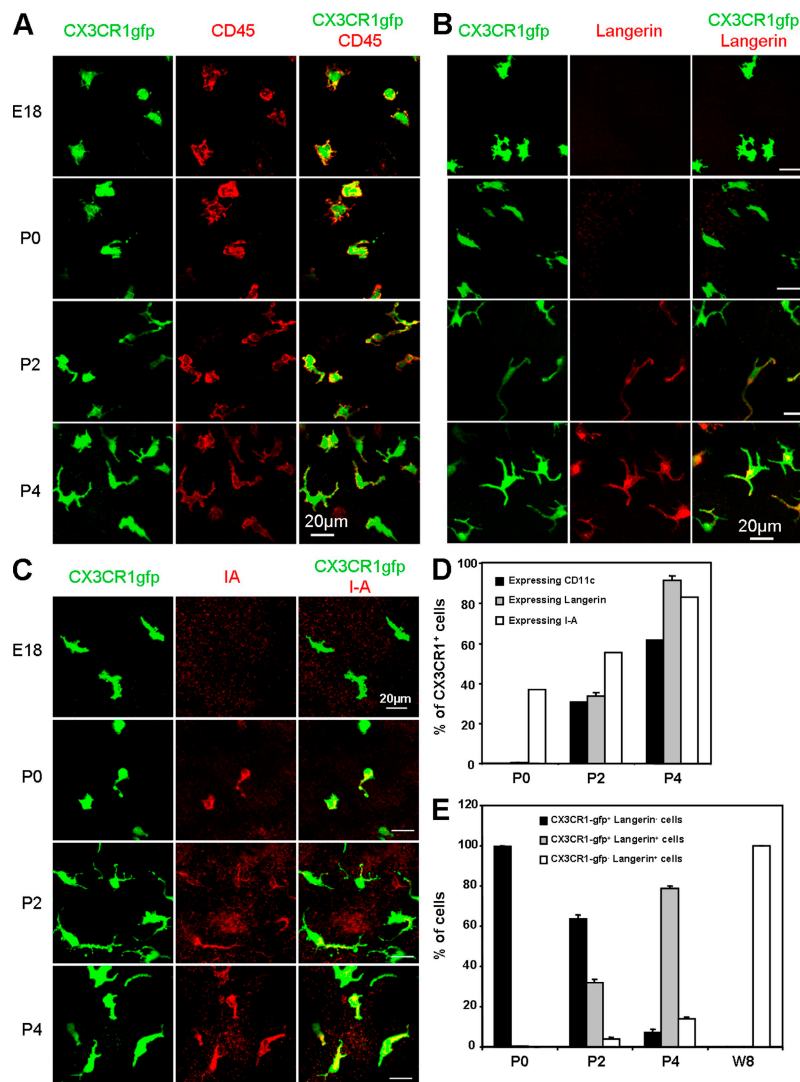

Figure 2. Epidermal CX$_3$CR1$^+$ CD45$^+$ myeloid precursors differentiate into langerin$^+$ MHCII$^+$ LCs between E18 and P2. Expression of (A) CD45, (B) langerin, and (C) MHCII. Maximal intensity projections of Z-stacks from epidermal sheets of CX$_3$CR1-GFP Rag$^{-/-}$ γc$^{-/-}$ mice at E18, P0, P2, and P4 are displayed. CX$_3$CR1-expressing cells are labeled in green and CD45, langerin, and MHCII are labeled in red using antibodies. Results are representative of 20 0.01-mm^2 Z-stacks per time point and per mouse (n = 3 mice per experimental time point). (D) Bar graph showing the percentage of epidermal CX$_3$CR1-GFP$^+$ cells expressing CD11c, langerin, or MHCII (I-A) at P0, P2, and P4. For each mouse, a range of 200–800 cells was analyzed. Means $\pm$ SD are displayed (n = 1–3 mice per experimental point). (E) Bar graph shows the percentage of epidermal cells expressing CX$_3$CR1 but not langerin, both CX$_3$CR1 and langerin, or langerin only at P0, P2, P4, and 8 wk. For each mouse, a range of 300–1,000 cells was analyzed. Means $\pm$ SD are displayed (n = 3–4 mice per experimental point).
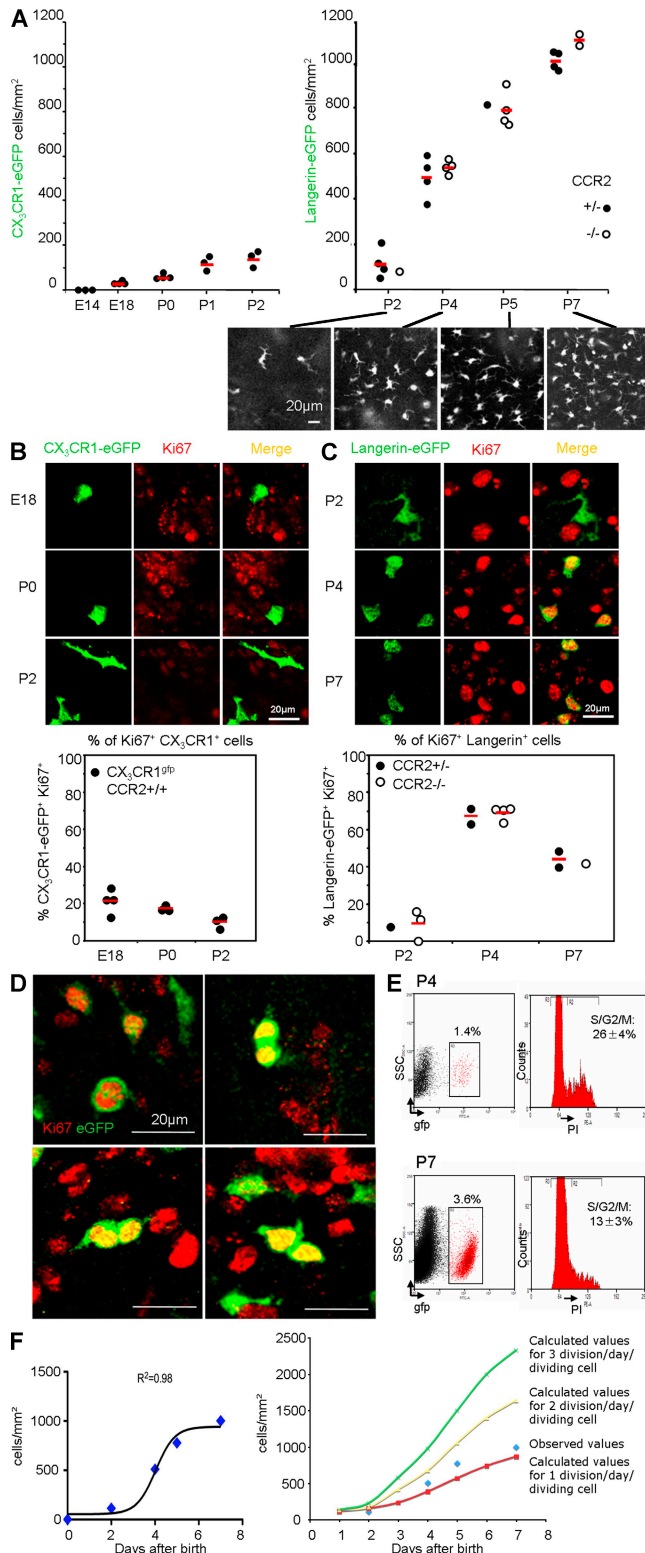
epidermis, we purified langerin[+] LCs from epidermal sheets from P4 and P7 langerin-GFP mice, and analyzed their DNA content using propidium iodide (PI). In P4 mice, 26 ± 4% of langerin-GFP cells contained >2N DNA, and were therefore in the S/G2/M phase of the cell cycle (Fig. 3 E and Fig. S4). The percentage of LCs in S/G2/M at day 7 was lower (13 ± 3%; Fig. 3 E). The results from PI staining are thus consistent with the kinetics of Ki67 staining and the mitotic figures observed in situ. As discussed, the drop in the percentage of CX$_3$CR1^{+} langerin^{−} cells observed in the epidermis between P2 and P4 (Fig. 2 B) indicates that the recruitment of new precursors is unlikely to contribute to the establishment of the LC network. In addition, we have used the least square methods to calculate the number of LCs per square millimeter that would be obtained between days 2 and 7 if each dividing LC (observed values using flow cytometry analysis of PI staining) was dividing once, twice, or three times per day in the absence of the recruitment of new precursors. This analysis indicated that dividing LCs must undergo between one and two divisions per day to fit our observed data (Fig. 3 F).

sents an individual mouse. (right) Kinetic of the number of langerin-GFP^{+} cells per square millimeter of the epidermis of langerin-GFP CCR2^{+/−} or langerin-GFP CCR2^{−/−} mice at various ages (P2, P4, P5, and P7). The epidermis was studied by intravital microscopy in live animals, as indicated in Materials and methods. LCs rapidly expand between P2 and P7. Each dot represents an individual mouse. Representative micrographs of maximal intensity projections of Z-stacks obtained at various time points are displayed below the graph. (B, top) Micrographs of epidermal sheets of CX$_3$CR1-GFP Rag^{−/−} γc^{−/−} mice at various ages (E18, P0, and P2). CX$_3$CR1^{+} cells are labeled in green and Ki67 is labeled in red. Images are optical slices from Z-stacks (optical zoom factor 2). (bottom) The graph shows the percentage of CX$_3$CR1^{+} cells expressing the nuclear proliferation marker Ki67 at various ages. For each mouse, a range of 100–500 cells was analyzed. Each dot represents an individual mouse. (C) Same as in B. Langerin-GFP CCR2^{+/−} or langerin-GFP CCR2^{−/−} mice at various ages (P2, P4, and P7) were analyzed. Horizontal lines represent means. (D) LC mitosis within the epidermis. Micrographs of langerin-GFP^{+} cells (green) expressing Ki67 (red) from epidermal sheets of P4 langerin-GFP mice. Pictures are optical slices from Z-stacks (optical zoom factor 2). Results are representative of six mice. For more information, see Fig. S3 and Video 1. (E) Cell-cycle analysis by PI staining of sorted P4 and P7 LCs by flow cytometry. Dot plots show the gate used for GFP-expressing LC sorting. Percentages of GFP^{+} cells among all events are indicated. Histograms show the cell-cycle analysis. Percentages of gated singlet PI[+] events in the S/G2/M phase are indicated. Means of three and two independent experiments ± SD at P4 and P7, respectively, are indicated. (F) Estimate of the duration of the langerin[+] cell-cycle during the first week of life. Using a nonlinear regression model (sigmoidal curve) based on data from A (R-squared value of the trend line = 0.98) and cell-cycle data from E, we formulated a polynomial regression model to extrapolate the percentage of cells proliferating at each day after birth (0–7 d), and we calculated the total number of cells per square millimeter over time that would be obtained considering one (red line), two (yellow line), or three (green line) divisions per day per dividing cell. Experimental data are represented by blue diamonds. The graph shows that experimental data fit with a model of in situ proliferation of LCs in which the length of the cell cycle is between 12 and 24 h. SSC, side scatter.

Figure 3. LCs expand in the epidermis by proliferating during the first week of life to establish an LC network. (A, left) Kinetic of the number of CX$_3$CR1^{+} cells per square millimeter of epidermis of CX$_3$CR1-GFP Rag^{−/−} γc^{−/−} mice at various ages (E14, E18, P0, P1, and P2). CX$_3$CR1^{+} cells appear slowly in the epidermis between E18 and P2. Cells were enumerated as indicated in Materials and methods. Each dot repre-

This fit well within the current understanding of the duration of the cell cycle in eukaryotic cells outside stem cells (Alberts et al., 2002), and thus, given their high proliferation index, a reasonable proliferation rate of langerin⁺ LCs is sufficient to explain their rapid increase in number.

Collectively, these data demonstrate that a single wave of CX_3CR1^+ $CD45^+$ langerin⁻ LC precursors enters the skin between E18 and P2 and differentiates into CX_3CR1^{low} $CD45^+$ langerin⁺ $MHCII^+$ $CD11c^+$ LCs, and then langerin⁺ LCs undergo a massive burst of proliferation during the first week of life, a result consistent with the observations by Chang-Rodriguez et al. (2005).

Proliferation of resident epidermal LC in the steady state

We next investigated whether LCs also proliferated in the adult epidermis. Analysis of large epidermal sheets from 4-, 8-,

and 14-wk-old langerin-GFP mice indicated that 5–7% of LCs expressed Ki67 (Fig. 4, A and B; and Video 2). The number of LCs in the steady state was not affected in $CCR2^{-/-}$ mice (Fig. 4 B). As exemplified by epidermal sheets from an 8-wk-old mouse (Fig. 4 A), Ki67⁺ cells were evenly distributed in the skin and did not seem to cluster around hair follicles. The distance between LCs and their closest neighbor was shorter in the case of pairs of Ki67⁺ LCs, which frequently formed doublets, suggesting that LCs may divide within the epidermis and that daughter cells migrate away from each other (Fig. 4, A and C). Indeed, three-dimensional reconstructions demonstrated langerin⁺ mitotic figures within the epidermis (Fig. 4 D, Video 3, and Video 4). Moreover, 5% of LCs from the epidermis of 10-wk-old mice were in the S/G2/M phase of the cell cycle based on PI staining (Fig. 4 E). Analysis of epidermal sheets from wild-type mice 7 wk after a bone marrow transplantation with
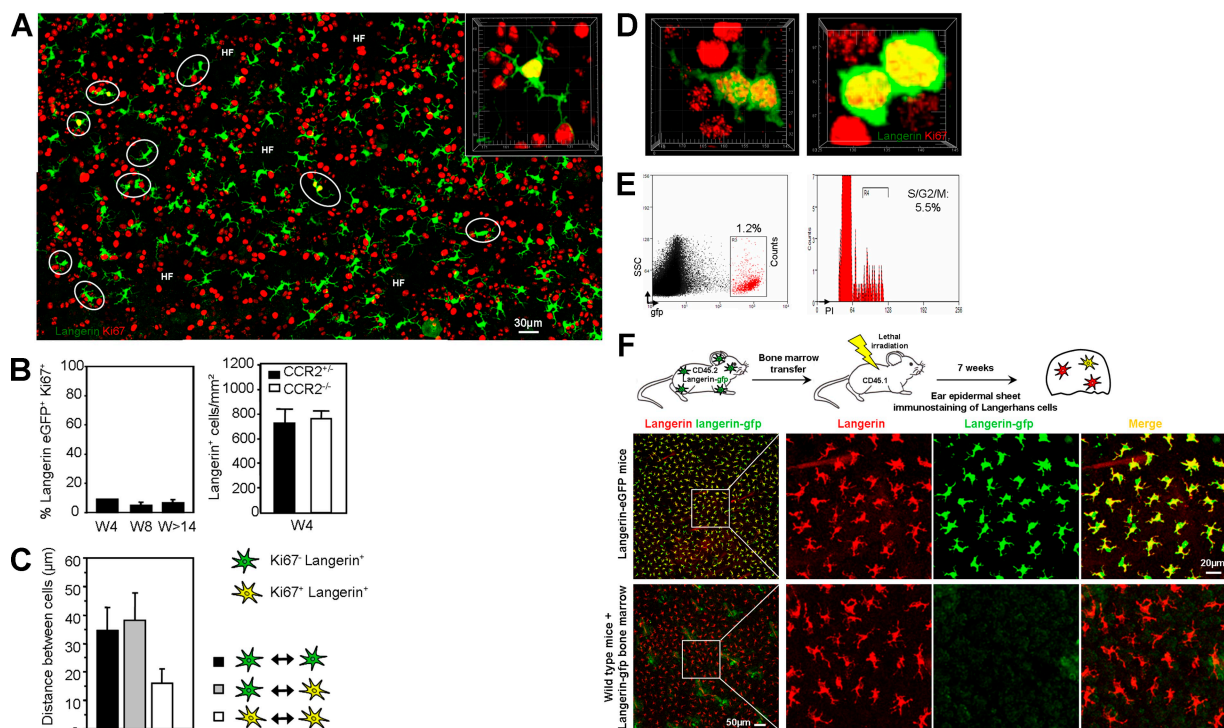

Figure 4. Proliferation of resident epidermal LCs in the steady state. (A) Tiled micrograph of ear epidermal sheets of a 8-wk-old langerin-GFP mouse. LCs are labeled in green and Ki67 is labeled in red. This tile has been obtained by assembling a series of maximal intensity projection Z-stacks. Ki67-expressing LCs are indicated with white circles. (inset) A three-dimensional reconstruction of a Ki67⁺ LC as in D (for more information see Video 2). Results are representative of epidermal sheets from four mice. (B, left) The percentage of Ki67⁺ langerin-GFP⁺ cells at various ages (W4, 4 wk; W8, 8 wk; W14, 14 wk). For each animal, 160–400 cells were analyzed. Means ± SD are displayed (n = 4 mice per experiment). (right) The number of langerin⁺ cells per square millimeter in the ear epidermis of littermate 4-wk-old $CCR2^{+/+}$ and $CCR2^{-/-}$ mice. Means of three experiments ± SD are displayed. (C) Graph shows the distance in micrometers between LCs and their closest neighbor. More than 600 langerin-GFP⁺ cells and >60 Ki67⁺ langerin-GFP⁺ cells were analyzed from the epidermis of 8-wk-old langerin-GFP⁺ mice. Similar results were obtained from the epidermis of 4- and 14-wk-old mice (n = 4). (D) Snapshots of a three-dimensional reconstruction of Z-stacks of 8-wk-old Ki67-expressing epidermal langerin-GFP⁺ cells using Imaris software. Results are representative of epidermal sheets from four mice. For more information, see Video 3 and Video 4. (E) Cell-cycle analysis by flow cytometry of sorted LCs as in Fig. 3 E. Percentages of gated singlet PI⁺ events in the S/G2/M phase are indicated. The experiments have been repeated three times with similar results. (F, top) CD45.1⁺ C57BL/6 recipient mice were irradiated (10 Gy) and injected with 10⁷ bone marrow cells obtained from adult langerin-GFP CD45.2⁺ mice to allow identification of donor-derived cells. 5 wk after transplantation, hematopoietic engraftment was analyzed by measurement of blood chimerism, and ears were collected 7 wk after transplantation. (bottom) Micrographs of epidermal sheets of control langerin-GFP mice and of irradiated chimeric mice. Langerin-GFP⁺ cells are labeled in green (anti-eGFP antibody) and langerin⁺ cells are labeled in red (antilangerin antibody). Maximal intensity projections from Z-stacks are displayed. Results are representative of epidermal sheets from four mice. HF, hair follicle; SSC, side scatter.

bone marrow cells from langerin-GFP mice confirmed previous findings (Merad et al., 2002) because all epidermal LCs were GFP⁻ (Fig. 4 F). Collectively, these data indicate that LCs continuously proliferate in the epidermis of mice.

Keratinocyte signals can drive a massive proliferation of LCs during skin inflammation

These findings raised the question of the mechanism involved in LC renewal during inflammation in the absence of radical depletion of LCs and/or of disruption of the epidermal basal membrane, such as that obtained with UV irradiation, genetic depletion, or graft-versus-host disease (GVHD; Bennett et al., 2005; Kaplan et al., 2005; Kissenpfennig et al., 2005; Merad et al., 2002). Treatment of mice with the vitamin D3 analogue MC903 induces the production of thymic stromal lymphopoietin (TSLP) by keratinocytes, which in turn is both required and sufficient to induce a skin and systemic inflammation that resembles human atopic dermatitis (AD; Li et al., 2006; Li et al., 2009). Akin to what is observed in humans, the epidermis of mice became thicker, and we observed that LC numbers were increased after 2 wk of treatment (Fig. 5, A and B). Analysis of Ki67 expression indicated a strong local proliferation of LCs with 25–35% of langerin⁺ Ki67⁺ cells (Fig. 5 C). Bone marrow chimera experiments indicated that only rare bone marrow–derived langerin cells could be detected in the epidermis of MC903-treated mice after 2 wk of treatment, and these cells were not proliferating (Fig. 5 D). We investigated whether MC903 acted directly on LCs by comparing LC proliferation in vitamin D receptor–deficient (VDR⁻ᐟ⁻) mice, in which all cells lack VDR (Fig. 5 E), and VDRᶠᐟᶠxK14-cre mice (VDRep⁻ᐟ⁻), in which keratinocytes but not LCs lack the receptor (Fig. 5 F). LC proliferation was completely dependent on VDR, indicating that LC proliferation is triggered in vivo by a keratinocyte signal that is transactivated by vitamin D and VDR. The keratinocyte signal is distinct from TSLP, because LC proliferation was comparable in TSLP⁻ᐟ⁻ mice and controls in the neonatal period, in adults in a steady state, and during MC903 treatment (Fig. S5). Of note, steady-state LC proliferation did not require VDR (Fig. 5 E). These findings also suggest that different mechanisms might be involved in LC production in adult animals depending on whether LCs are previously depleted and/or the epidermal basal membrane is disrupted (as with UV irradiation, genetic depletion, and GVHD; Merad et al., 2002; Bennett et al., 2005; Kaplan et al., 2005; Kissenpfennig et al., 2005), or if LC expansion is induced in an LC–replete animal with an "intact" skin.

Human epidermal LCs proliferate in the steady state, and proliferation is increased in two patients with AD

Ki67⁺ langerin⁺ cells were also present in epidermal sheets from healthy human donors, where they accounted for 2–4% of epidermal LCs, suggesting that human epidermal LCs also proliferate within the epidermis, as proposed earlier (Fig. 6, A–C; and Video 5; Czernielewski and Demarchez, 1987).

We obtained epidermal sheets from the skin of two patients with AD. Ki67⁺ langerin⁺ cells accounted for 13 and 16% of epidermal LCs (Fig. 6, C and D), suggesting that proliferation of LCs is also increased in humans with AD. Although the precise role of LCs in allergic diseases is still debated, a concordant increase in LC proliferation in patients with human AD and in a mouse model for the disease suggests a potential relevance for the pathophysiology of the disease.

DISCUSSION

Our results indicate that although monocytes and classical DCs constantly renew from a proliferating bone marrow MDP (Fogg et al., 2006; Liu et al., 2009), LCs renew from the proliferation of resident, differentiated LCs. CD115⁺ CD135⁻ CD11b⁺ CD45⁺ CX₃CR1⁺ LC precursors enter the skin before birth as a single wave of recruitment around E18. These precursors, evenly distributed in the epidermis, differentiate into LCs expressing langerin, MHCII, and CD11c between P0 and P4. Langerin⁺ LCs then undergo a burst of proliferation that increases their numbers by >10-fold and establishes the LC network. In contrast to our observations, results published by Bennett et al. (2005), Kaplan et al. (2007), and Poulin et al. (2007) show that after genetic depletion, LCs first appear in clusters, and the replenishment of genetically depleted mice is very slow and takes up to 7 wk. This may be because in this model rare and scattered precursors are responsible for LC replenishment. In contrast, the absence of clusters and the fast development of the network during the first week of life in the physiological condition, as we describe in this study, can easily be explained by the high number and the even distribution of precursors present at birth.

According to our data, the LC network appears to be maintained throughout life by slow proliferation of epidermal langerin⁺ LCs rather than from a dermal or hair follicle precursor, as previously proposed (Merad et al., 2008). Moreover, a surprising result from this study is that the resident langerin⁺ LCs can indeed be induced to massively proliferate by a keratinocyte signal in adults, showing that epidermal LCs can expand in the epidermis independently of a bone marrow input in a steady state as well as during inflammation. These results differ markedly from observations after UV treatment and during GVHD, when bone marrow–derived langerin⁺ cells were observed, using flow cytometry, to replace LCs in the epidermis (Merad et al., 2002; Ginhoux et al., 2006). However, it is at this time difficult to compare AD with the UV and GVHD models. In UV treatment and GVHD, LCs are killed, which makes it difficult to study their proliferation, and the dermis is heavily infiltrated by bone marrow–derived inflammatory cells, which can express langerin and can infiltrate the upper dermis and epidermis.

Collectively, the present data suggest a new model for the renewal of resident cells in which a single wave of progenitors seeds tissue and differentiates before proliferating to establish a population of resident cells that will reenter the cell cycle to ensure homeostasis and expansion, when required, based on signals from the microenvironment (Fig. 7). It remains to be

studied whether all LCs will keep the ability to proliferate during adult life or if proliferation is caused by a subset of langerin[+] LCs. In situ fate mapping experiments of individual

cells will be required to answer this question. However, the high index of proliferation observed during inflammation (30% of LCs staining with anti–Ki67 antibodies) suggests that
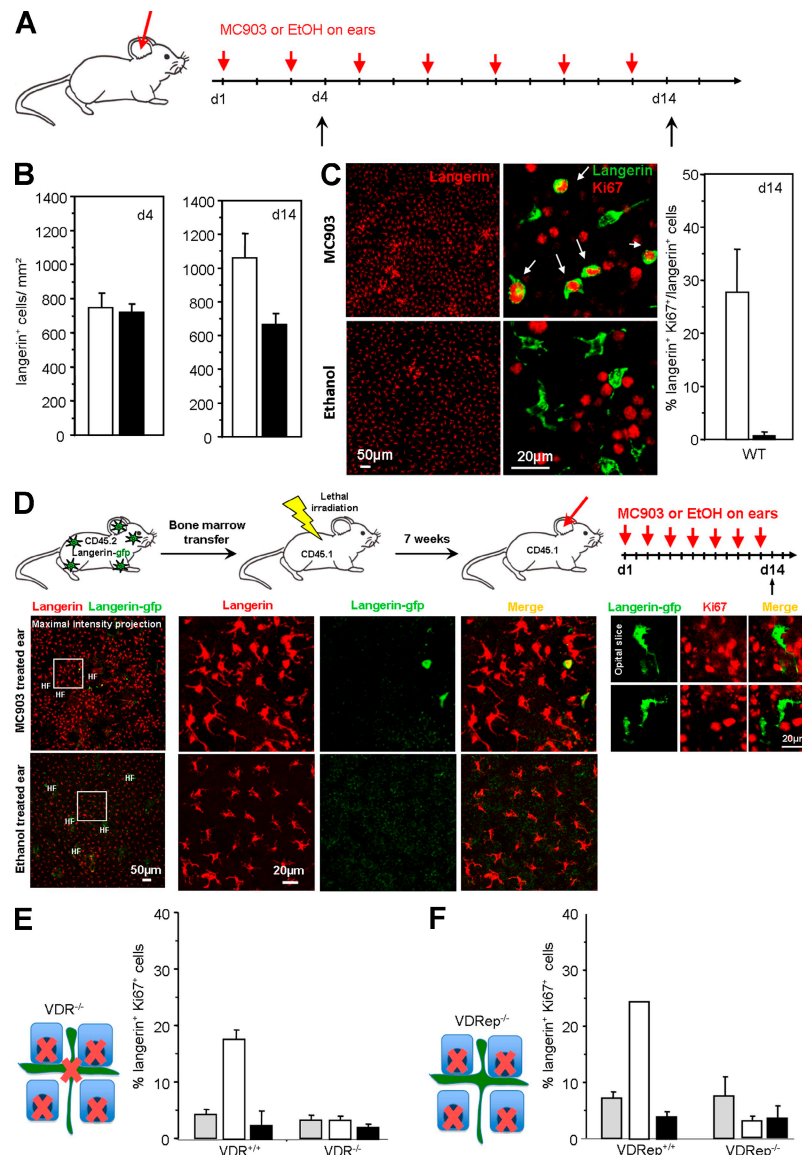
Figure 5. A keratinocyte–derived signal can drive a massive proliferation of LCs during skin inflammation. (A) Time course of treatment of the ears of mice with MC903 or ethanol. Analysis of the epidermis was performed at days 4 and 14. (B) Graphs show the number of langerin^{+} cells per square millimeter in the epidermis of wild-type mice treated with MC903 (white) or ethanol (black). Means ± SD are displayed (*n* = 3). (C) Micrographs are representative maximal intensity projections (left) or optical slices (right) of Z-stacks from epidermal sheets of mice treated for 14 d. Langerin^{+} cells are either labeled in red (left) or in green (right), and Ki67 is labeled in red (right). Results are representative of epidermal sheets from two to three animals. The graph shows the percentage of langerin^{+} cells expressing Ki67 after 14 d of MC903 (white) or ethanol (black) treatment. For each animal, 150–300 langerin^{+} cells were analyzed. Means of two to three experiments ± SD are displayed. (D) Similar to the experiment described in Fig. 4 F. 7 wk after transplantation, MC903 or ethanol was applied on the ear every other day for 14 d. Micrographs show epidermal sheets from MC903-treated ears (top) or epidermal sheets from control ethanol-treated ears (bottom). (left) Langerin-GFP^{+} cells are labeled in green (anti-eGFP antibody) and langerin^{+} cells are labeled in red (antilangerin antibody). Maximal intensity projections from Z-stacks are shown. Results are representative of 10 0.56-mm² Z-stacks per mice. The pictures show few (<1%) bone marrow–derived LCs recruited in the epidermis of MC903-treated mice after 2 wk of treatment. (right) Langerin-GFP^{+} cells (green) are not labeled with Ki67 (red). The pictures show two representative examples of langerin-GFP^{+} cells recruited in the epidermis after MC903 treatment. For each animal, >500 Ki67^{+} cells were analyzed. (E) Treatment of VDR^{−/−} mice with MC903 or ethanol. Mice were treated with MC903 or ethanol as in A, and analysis of the epidermis was performed at day 14. The bar graph represents the percentage of langerin^{+} cells expressing Ki67 in VDR^{+/+} or VDR^{−/−} mice either untreated (gray bar) or treated for 14 d with MC903 (white bar) or ethanol (black bar). For each animal, 250–600 langerin^{+} cells were analyzed. Means of two experiments ± SD are displayed. (F) Similar to the experiment described in E but performed on VDRep^{+/+} and VDRep^{−/−} mice. HF, hair follicle.

the fraction of LCs that keeps the potential to enter the cell cycle must be relatively high.

The present results thus indicate that the microenvironment of LCs, e.g., keratinocyte signals, is likely to play a major role in the control of LC homeostasis, in line with the ability of keratinocytes to produce M-CSF and TGF-β1, which have been shown to be required for the development of the LC network (Chodakewitz et al., 1990; Borkowski et al., 1996; Ginhoux et al., 2006; Kaplan et al., 2007). Other cytokines are involved in LC biology, such as TLSP and RANKL (Barbaroux et al., 2008), but our data do not support a major role for TSLP in the control of LC proliferation during development and inflammation.

The alternative pathway for the development and renewal of mononuclear phagocytes that we describe in this paper may be useful in organs, such as the epidermis, that lack blood vessels and are not sites of active leukocyte extravasation, or that must be protected against the entry of inflammatory cells. Notably, as brain microglia also renew independently of the bone marrow (Ajami et al., 2007; Mildner et al., 2007), it will be interesting to investigate if a similar mechanism is responsible for the development and homeostasis of microglia.

The precise role of LCs in the immune response, particularly in allergic diseases such as AD, is still debated. A recent study proposed that LCs are important for the development of this disease (Elentner et al., 2009). The concordant increase in LC proliferation in human AD and a mouse model for the disease observed in our study may suggest that LC proliferation is of physiological relevance in this allergic disease. Finally, among outstanding questions, the origin of the epidermal LC precursor and the mechanisms by which it enters the epidermis around E18 are not known.

It is possible that the precursors recruited in the epidermis around E18 originate from bone marrow–derived cells, such as MDPs, after the location of fetal hematopoiesis begins to switch from the fetal liver to fetal bone marrow at E15 (Wolber et al., 2002; Bertrand et al., 2005). It is also possible that the epidermal precursor originates from the CX_3CR1^+ cells that we have detected in the dermis of fetuses at E14 (Fig. 1 A) and that may derive from the fetal liver or yolk sack. Adoptive transfer of
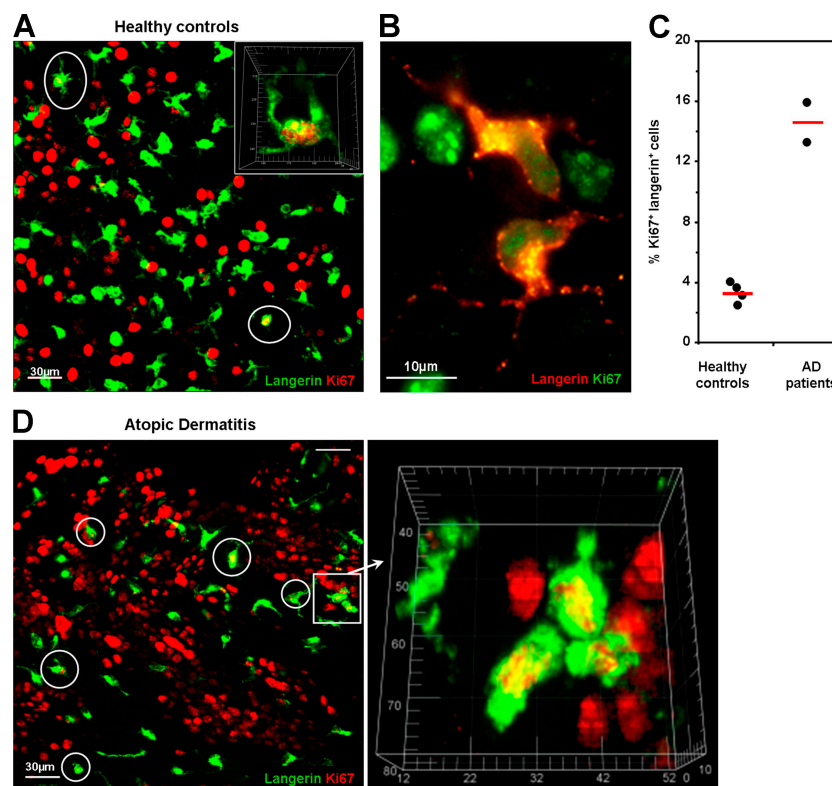

Figure 6. Proliferation of human LCs in the epidermis from healthy controls and AD patients. Epidermal sheets were obtained from four healthy donors and two AD patients and analyzed by confocal microscopy for expression of langerin (green) and Ki67 (red). (A) Representative maximal intensity projections of Z-stacks of healthy epidermis. Ki67+/langerin+ LCs are circled in white, and nuclear localization of Ki67 was confirmed by three-dimensional visualization (for more information see Video 5). (B) Ki67+ LC doublets were detected in human epidermis. (C) A significantly higher percentage of Ki67+ LCs was observed in AD epidermis compared with healthy controls (14.5 ± 1.55% and 3.21 ± 0.33%, respectively; P = 0.003 ; n = 2 and 4, respectively). A minimum of 500 LCs, as visualized by langerin expression, were analyzed per healthy donor and patient. Results are expressed as mean percentages of Ki67+LCs ± SD. (D) Representative maximal intensity projections of Z-stacks of epidermis from AD patients. A group of three Ki67+ LCs is shown as a three-dimensional reconstruction. Ki67+/langerin+ LCs are circled in white. The scale is graduated in micrometers.
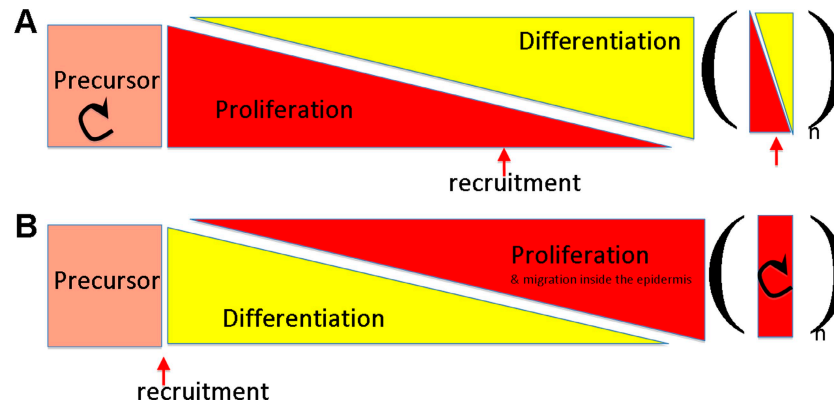
Figure 7.   Comparison of the classical model of myeloid cell homeostasis and LC homeostasis. (A) Classical model for cell proliferation and differentiation. Precursors are located in a niche (e.g., the bone marrow), self-renew, and give rise to proliferating committed progenitors and precursors. Precursors with a limited differentiation potential migrate to the peripheral tissue and complete their differentiation. During the life of the animal, when differentiated cells die, new precursors will migrate from the bone marrow to replace them. (B) LC precursors are recruited into the epidermis as a single wave before birth and differentiate in situ, and then proliferate to form a network. No further input from the progenitors is needed. During life, differentiated cells can enter the cell cycle when required.

putative precursors into fetuses and embryos will help answer this question, but it may be a difficult experiment.

MATERIALS AND METHODS

Animals. CX_3CR1-GFP $Rag^{-/-}$ $\gamma c^{-/-}$ (Auffray et al., 2007), langerin-GFP (Kissenpfennig et al., 2005), $VDR^{-/-}$, $VDRep^{-/-}$, and $TSLP^{-/-}$ mice (Li et al., 2006; Li et al., 2009) have been previously described. $CCR2^{-/-}$ mice were provided by I. Charo (Gladstone Institute of Cardiovascular Disease, University of California, San Francisco, San Francisco, CA). Mice were maintained in specific pathogen-free animal facilities at the University Paris-Descartes, King's College London, Institut de Génétique et de Biologie Moléculaire et Cellulaire, and Institut Biologie Moléculaire et Cellulaire (Strasbourg, France). All animal protocols were approved by the Institutional Committees on Animal Welfare of the University Paris-Descartes and of the United Kingdom Home Office.

Preparation and immunolabeling of mice epidermal sheets. Mice of defined ages, ranging from E14 to P7, were sacrificed. Ventral skin was dissected, cut into 1 × 1–cm pieces, and placed dermal side down on PBS 20 mM EDTA for 2 h at 37°C. The epidermis was then peeled off the dermis. For E14 fetuses, whole skin was processed. To prepare epidermal sheets from adult mice (4–14 wk old), the ventral and dorsal halves of ears were split. To separate the epidermis and dermis, both halves were placed dermal side down on PBS 0.2% trypsin (Invitrogen) for 25 min at 37°C. In some experiment, PBS 0.5 M ammonium thiocyanate (Sigma–Aldrich) was used to separate the epidermis and dermis with a 40-min incubation at 37°C.

The epidermal sheets were fixed with PBS 3% paraformaldehyde, washed, and permeabilized in PBS 0.5% Triton X-100 (Sigma–Aldrich) for 15 min. Sheets were blocked by normal goat IgG (Invitrogen) in PBS 0.5% Triton X-100 (staining buffer) for 30 min before overnight labeling with rat anti–mouse Ki67 (clone TEC-3; Dako), CD45 (clone 30-F11; BD), langerin (clone 929F3.01; Dendritics), I-A/I-E (clone 2G9; BD), or rat anti–hamster CD11c (clone HL3; BD) antibodies. Samples were washed and incubated with Cy3-conjugated goat anti–rat or Cy3-conjugated goat anti–hamster antibodies (Jackson ImmunoResearch Laboratories, Inc.). To avoid antibody cross-reactions, sheets were blocked with staining buffer supplemented with normal rat IgG (Invitrogen) and further labeled with either rabbit anti-eGFP (Invitrogen) or rabbit antilangerin (clone M-200; Santa Cruz Biotechnology, Inc.). Samples were washed and labeled with Alexa Fluor 488–conjugated goat anti–rabbit (Invitrogen). Sheets were mounted in mounting medium (Vector Laboratories) complemented with DAPI (diluted 1:1,000; Invitrogen) for nuclei staining.

For hematoxylin and eosin (H&E) staining, whole embryos were fixed for 1 wk in neutral buffer formalin (Genta Medical) before paraffin embedding. 6-µm sections were labeled with H&E. After mounting, embryo sections were imaged using a microscope (Axiophot; Carl Zeiss, Inc.).

Preparation and immunostaining of human epidermal sheet. 6-mm punch skin biopsies from four healthy donors and two AD patients (non–steroid treated) were obtained after informed consent and approved by the St. Thomas' Hospital Research Ethics Committee (reference number 06/Q0702/138), and were incubated for 2 h at 37°C in PBS containing 20 mM EDTA. The epidermis was separated from the underlying dermis using forceps and washed several times in PBS. Epidermal sheets were fixed in PBS with 4% formaldehyde at 4°C for 45 min and subsequently washed in PBS. Sheets were stained overnight at room temperature in 500 µl PBS 0.25% Triton X-100 with anti-Ki67 antibody (diluted 1:500; Abcam) and anti–human langerin-PE antibody (diluted 1/10; Coulter Immunotech). Samples were washed twice in PBS 0.1% Tween and incubated for an additional 2 h at room temperature in 300 µl PBS 0.25% Triton X-100 with goat anti–rabbit Alexa Fluor 488 antibody (diluted 1:300; Invitrogen) and donkey anti–mouse IgG1 Cy3 (diluted 1:300; Jackson ImmunoResearch Laboratories, Inc.) before mounting.

Image acquisition and quantitative analysis. All Z-stack acquisitions were done using a confocal microscope (SP5; Leica) with 20× and 40× lenses. The number of LCs per square millimeter of epidermis was determined by acquiring Z-stacks of immunolabeled epidermal sheets. A minimum of four Z-stacks (0.56 mm^2/Z-stack) were acquired per epidermal sheet. The number of cells per Z-stack was enumerated and represented as cells per square millimeter. The distance between a langerin-GFP$^+$ cell and its closest GFP$^+$ neighbor (Ki67$^+$ or Ki67$^-$) was measured on a maximal intensity projection of Z-stacks of immunolabeled epidermal sheets. All image quantification and rendering was performed on MetaMorph (MDS Analytical Technologies) and Imaris (Bitplane) software.

Intravital microscopy. Langerin-GFP CCR2$^{+/-}$ or CCR2$^{-/-}$ mice of various ages (P2–P7) were anesthetized using 25 mg/kg ketamine, 5 mg/kg xylazine, and 0.8 mg/kg acepromazine injected intraperitoneally. Mice were kept at 37°C with oxygen (0.5 liter/min). Mice abdomens were placed on a custom–made tray-stage insert with a circular 2.5-cm hole covered with a coverslip. Images were acquired using an inverted confocal microscope (LSM 510; Carl Zeiss, Inc.) equipped with a 20×/0.75 Plan Apochromat objective. A thermostated chamber (Carl Zeiss, Inc.) was used to keep the microscope, mouse, tray, and objective at 37°C during the experiment.

Z-stacks (with 1-µm Z-spacing) were acquired on the ventral skin (at least seven Z-stacks per mouse, 0.22 mm²/Z-stack), and the number of langerin-GFP⁺ cells per square millimeter was determined.

LC isolation, PI staining, and cell-cycle analysis. Skin from langerin-GFP neonates (P4 and P7) and split ears of 10-wk-old mice were incubated in PBS 0.2% trypsin at 37°C for either 1 h or 25 min, respectively. The epidermis was peeled from the dermis and reincubated for 2 h in PBS with 1 mg/ml collagenase D (Roche). An epidermal cell suspension was obtained by mechanical dissociation of epidermal sheets on a 100-µm cell strainer (BD). GFP-expressing LCs were sorted (FACSAria II; BD). Sorted cells were washed with PBS and fixed in 70% ethanol at 4°c for 30 min. After washes, samples were stained with 50 µg/ml PI (Invitrogen) complemented with 50 µg/ml RNaseA (Sigma-Aldrich) at 37°C for 20 min. Samples were analyzed by flow cytometry (FACSAria II). The sorting and cell-cycle analyses were performed as described in Fig. S4.

Antibodies used for flow cytometry. The following purified or conjugated antibodies were purchased from BD: purified anti-FcγRIII/II (CD32/16; clone 2.4G2), PECy7- or biotin-labeled anti-CD11b (M1/70), allophycocyanin (APC)-labeled anti-CD117 (c-kit; 2B8), biotin-labeled anti-NK1.1 (PK136), biotin- or APC-labeled anti-CD11c (HL3), PECy7- and biotin-labeled anti-CD3 (145-2C11), PECy7- and biotin-labeled anti-CD19 (MB19-1), biotin-labeled anti–I-A/I-E (2G9), PE-labeled anti–I-Aᵇ(AF6-120.1), and biotin-labeled anti-Lyc6 (AL-21). The following antibodies were purchased from eBioscience: PE-labeled anti-Flt3 (A2F10), PE- or biotin-labeled anti-CD115 (AFS98), and PECy7- and biotin-labeled anti-CD127 (A7R34). Antibodies used for depletion, including TER-119 (erythrocytes) and RB6-8C5 (Ly6-C/G), were supernatants of hybridomas donated by B. Rocha (Institut Fédératif de Recherche Necker, Paris, France). Streptavidin Pacific blue was purchased from Invitrogen.

Phenotyping of bone marrow MDPs and CDPs, and epidermal CX₃CR1-GFP⁺ and langerin-GFP⁺ cells. BM cells from femurs and tibias of CX₃CR1-GFP Rag⁻/⁻ γc⁻/⁻ mice aged 6–8 wk were flushed with serum-free RPMI 1640. For isolation of MDPs and CDPs, BM granulocytes and erythrocytes were labeled with RB6-8C5 and TER-119, respectively, and depleted using sheep anti–rat Dynabeads (Invitrogen). Fc receptors were blocked with antibody to FcγRIII/II (2.4G2), and cells were labeled using antibodies against lineage markers (IL-7Rα, CD11b, NK1.1, CD3, and CD19), CD117, CD115, CD135, CD11c, and I-A.

Epidermal cells from E18 CX₃CR1-GFP Rag2⁻/⁻ γc⁻/⁻ embryos and 8-wk-old langerin-GFP mice were isolated with a similar protocol. Fc receptors were blocked with antibody to FcγRIII/II (2.4G2), and cells were labeled using antibodies against CD11b, CD117, CD115, CD135, CD11c, I-A, and Lyc6. MDPs (defined as GFP⁺ [CX₃CR1] lineage⁻ CD117⁺), CDPs (defined as lineage⁻ CD135⁺ CD117^low), and epidermal CX₃CR1-GFP⁺ and langerin-GFP⁺ cells were analyzed by flow cytometry using a FACSAria II. Flow cytometry data were analyzed using Summit software (version 4.3; Dako).

In vivo induction of AD. Induction of AD by topical application of MC903 (a low calcemic analogue of vitamin D) was performed as previously described (Li et al., 2006; Li et al., 2009). In summary, 10–14-wk-old mice were treated every other day with 1 nmol of MC903 diluted in 25 µl ethanol on the right ear and treated with the same volume of ethanol on the left ear as a control. Immunolabeled epidermis were then analyzed after 4 and 14 d of treatment.

Online supplemental material. Fig. S1 illustrates the decrease in LC size between P2 and P7 as examined by intravital microscopy. Fig. S2 shows that Ki67⁺ CX₃CR1⁺ cells can be detected in the epidermis of E18 fetuses. Fig. S3 illustrates examples of mitosis of LCs within the epidermis of 4-d-old neonates. Fig. S4 shows the protocol followed for the analysis of DNA content of LCs by flow cytometry. Fig. S5 displays data indicating that TSLP deficiency does not affect LC proliferation. Videos 1–4 show three-dimensional reconstructed Z-stacks of epidermal langerin-GFP⁺ cells (green) expressing the proliferation nuclear factor Ki67 (red) in the epidermis of a mouse at day 4 after birth (Video 1) and 8-wk-old mice (Videos 2, 3, and 4). Video 5 shows three-dimensional reconstructed Z-stacks of human epidermal langerin⁺ cells (green) expressing the proliferation nuclear factor Ki67 (red) in the epidermis of a healthy human donor. Nuclei are labeled in blue. Online supplemental material is available at http://www.jem.org/cgi/content/full/jem.20091586/DC1.

REFERENCES

Ajami, B., J.L. Bennett, C. Krieger, W. Tetzlaff, and F.M. Rossi. 2007. Local self-renewal can sustain CNS microglia maintenance and function throughout adult life. *Nat. Neurosci.* 10:1538–1543. doi:10.1038/nn2014

Alberts, B., A. Johnson, J. Lewis, M. Raff, K. Roberts, and P. Walter. 2002. Molecular Biology of the Cell. 4th edition. Garland Science, New York. 1616 pp.

Asli, B., O. Lantz, J.P. DiSanto, S. Saeland, and F. Geissmann. 2004. Roles of lymphoid cells in the differentiation of Langerhans dendritic cells in mice. *Immunobiology*. 209:209–221. doi:10.1016/j.imbio.2004.05.002

Auffray, C., D. Fogg, M. Garfa, G. Elain, O. Join-Lambert, S. Kayal, S. Sarnacki, A. Cumano, G. Lauvau, and F. Geissmann. 2007. Monitoring of blood vessels and tissues by a population of monocytes with patrolling behavior. *Science*. 317:666–670. doi:10.1126/science.1142883

Auffray, C., D.K. Fogg, E. Narni-Mancinelli, B. Senechal, C. Trouillet, N. Saederup, J. Leemput, K. Bigot, L. Campisi, M. Abitbol, et al. 2009. CX3CR1⁺ CD115⁺ CD135⁺ common macrophage/DC precursors and the role of CX3CR1 in their response to inflammation. *J. Exp. Med*. 206:595–606. doi:10.1084/jem.20081385

Barbaroux, J.B., M. Beleut, C. Brisken, C.G. Mueller, and R.W. Groves. 2008. Epidermal receptor activator of NF-kappaB ligand controls Langerhans cells numbers and proliferation. *J. Immunol*. 181:1103–1108.

Bennett, C.L., E. van Rijn, S. Jung, K. Inaba, R.M. Steinman, M.L. Kapsenberg, and B.E. Clausen. 2005. Inducible ablation of mouse Langerhans cells diminishes but fails to abrogate contact hypersensitivity. *J. Cell Biol*. 169:569–576. doi:10.1083/jcb.200501071

Bennett, C.L., M. Noordegraaf, C.A. Martina, and B.E. Clausen. 2007. Langerhans cells are required for efficient presentation of topically applied hapten to T cells. *J. Immunol*. 179:6830–6835.

Bertrand, J.Y., A. Jalil, M. Klaine, S. Jung, A. Cumano, and I. Godin. 2005. Three pathways to mature macrophages in the early mouse yolk sac. *Blood*. 106:3004–3011. doi:10.1182/blood-2005-02-0461

Borkowski, T.A., J.J. Letterio, A.G. Farr, and M.C. Udey. 1996. A role for endogenous transforming growth factor β1 in Langerhans cell biology: the skin of transforming growth factor β1 null mice is devoid of epidermal Langerhans cells. *J. Exp. Med*. 184:2417–2422. doi:10.1084/jem.184.6.2417

Chang-Rodriguez, S., W. Hoetzenecker, C. Schwärzler, T. Biedermann, S. Saeland, and A. Elbe-Bürger. 2005. Fetal and neonatal murine skin harbors Langerhans cell precursors. *J. Leukoc. Biol*. 77:352–360. doi:10.1189/jlb.1004584

Chodakewitz, J.A., J. Lacy, S.E. Edwards, N. Birchall, and D.L. Coleman. 1990. Macrophage colony-stimulating factor production by murine and human keratinocytes. Enhancement by bacterial lipopolysaccharide. *J. Immunol*. 144:2190–2196.

Czernielewski, J.M., and M. Demarchez. 1987. Further evidence for the self-reproducing capacity of Langerhans cells in human skin. *J. Invest. Dermatol.* 88:17–20. doi:10.1111/1523-1747.ep12464659

Czernielewski, J., P. Vaigot, and M. Prunièras. 1985. Epidermal Langerhans cells–a cycling cell population. *J. Invest. Dermatol.* 84:424–426. doi:10.1111/1523-1747.ep12265523

de Witte, L., A. Nabatov, M. Pion, D. Fluitsma, M.A. de Jong, T. de Gruijl, V. Piguet, Y. van Kooyk, and T.B. Geijtenbeek. 2007. Langerin is a natural barrier to HIV-1 transmission by Langerhans cells. *Nat. Med.* 13:367–371. doi:10.1038/nm1541

Elbe, A., E. Tschachler, G. Steiner, A. Binder, K. Wolff, and G. Stingl. 1989. Maturational steps of bone marrow–derived dendritic murine epidermal cells. Phenotypic and functional studies on Langerhans cells and Thy-1+ dendritic epidermal cells in the perinatal period. *J. Immunol.* 143:2431–2438.

Elentner, A., D. Finke, M. Schmuth, S. Chappaz, S. Ebner, B. Malissen, A. Kissenpfennig, N. Romani, and S. Dubrac. 2009. Langerhans cells are critical in the development of atopic dermatitis-like inflammation and symptoms in mice. *J. Cell. Mol. Med.* 10.1111/j.1582-4934.2009.00797.x.

Fogg, D.K., C. Sibon, C. Miled, S. Jung, P. Aucouturier, D.R. Littman, A. Cumano, and F. Geissmann. 2006. A clonogenic bone marrow progenitor specific for macrophages and dendritic cells. *Science.* 311:83–87. doi:10.1126/science.1117729

Frelinger, J.A., and J.G. Frelinger. 1980. Bone marrow origin of Ia molecules purified from epidermal cells. *J. Invest. Dermatol.* 75:68–70. doi:10.1111/1523-1747.ep12521247

Geissmann, F., C. Prost, J.P. Monnet, M. Dy, N. Brousse, and O. Hermine. 1998. Transforming growth factor β1, in the presence of granulocyte/macrophage colony-stimulating factor and interleukin 4, induces differentiation of human peripheral blood monocytes into dendritic Langerhans cells. *J. Exp. Med.* 187:961–966. doi:10.1084/jem.187.6.961

Giacometti, L., and W. Montagna. 1967. Langerhans cells: uptake of tritiated thymidine. *Science.* 157:439–440. doi:10.1126/science.157.3787.439

Gilliam, A.C., I.B. Kremer, Y. Yoshida, S.R. Stevens, E. Tootell, M.B. Teunissen, C. Hammerberg, and K.D. Cooper. 1998. The human hair follicle: a reservoir of CD40+ B7-deficient Langerhans cells that repopulate epidermis after UVB exposure. *J. Invest. Dermatol.* 110:422–427. doi:10.1046/j.1523-1747.1998.00162.x

Ginhoux, F., F. Tacke, V. Angeli, M. Bogunovic, M. Loubeau, X.M. Dai, E.R. Stanley, G.J. Randolph, and M. Merad. 2006. Langerhans cells arise from monocytes in vivo. *Nat. Immunol.* 7:265–273. doi:10.1038/ni1307

Kanitakis, J., P. Petruzzo, and J.M. Dubernard. 2004. Turnover of epidermal Langerhans' cells. *N. Engl. J. Med.* 351:2661–2662. doi:10.1056/NEJM200412163512523

Kaplan, D.H., M.C. Jenison, S. Saeland, W.D. Shlomchik, and M.J. Shlomchik. 2005. Epidermal langerhans cell-deficient mice develop enhanced contact hypersensitivity. *Immunity.* 23:611–620. doi:10.1016/j.immuni.2005.10.008

Kaplan, D.H., M.O. Li, M.C. Jenison, W.D. Shlomchik, R.A. Flavell, and M.J. Shlomchik. 2007. Autocrine/paracrine TGFβ1 is required for the development of epidermal Langerhans cells. *J. Exp. Med.* 204:2545–2552. doi:10.1084/jem.20071401

Katz, S.I., K. Tamaki, and D.H. Sachs. 1979. Epidermal Langerhans cells are derived from cells originating in bone marrow. *Nature.* 282:324–326. doi:10.1038/282324a0

Kissenpfennig, A., S. Henri, B. Dubois, C. Laplace-Builhé, P. Perrin, N. Romani, C.H. Tripp, P. Douillard, L. Leserman, D. Kaiserlian, et al. 2005. Dynamics and function of Langerhans cells in vivo: dermal dendritic cells colonize lymph node areas distinct from slower migrating Langerhans cells. *Immunity.* 22:643–654. doi:10.1016/j.immuni.2005.04.004

Larregina, A.T., A.E. Morelli, L.A. Spencer, A.J. Logar, S.C. Watkins, A.W. Thomson, and L.D. Falo Jr. 2001. Dermal-resident CD14+ cells differentiate into Langerhans cells. *Nat. Immunol.* 2:1151–1158. doi:10.1038/ni731

Li, M., P. Hener, Z. Zhang, S. Kato, D. Metzger, and P. Chambon. 2006. Topical vitamin D3 and low-calcemic analogs induce thymic stromal lymphopoietin in mouse keratinocytes and trigger an atopic dermatitis. *Proc. Natl. Acad. Sci. USA.* 103:11736–11741. doi:10.1073/pnas.0604575103

Li, M., P. Hener, Z. Zhang, K.P. Ganti, D. Metzger, and P. Chambon. 2009. Induction of thymic stromal lymphopoietin expression in keratinocytes is necessary for generating an atopic dermatitis upon application of the active vitamin D3 analogue MC903 on mouse skin. *J. Invest. Dermatol.* 129:498–502. doi:10.1038/jid.2008.232

Liu, K., C. Waskow, X. Liu, K. Yao, J. Hoh, and M. Nussenzweig. 2007. Origin of dendritic cells in peripheral lymphoid organs of mice. *Nat. Immunol.* 8:578–583. doi:10.1038/ni1462

Liu, K., G.D. Victora, T.A. Schwickert, P. Guermonprez, M.M. Meredith, K. Yao, F.F. Chu, G.J. Randolph, A.Y. Rudensky, and M. Nussenzweig. 2009. In vivo analysis of dendritic cell development and homeostasis. *Science.* 324:392–397. doi:10.1126/science.1171243

Merad, M., M.G. Manz, H. Karsunky, A. Wagers, W. Peters, I. Charo, I.L. Weissman, J.G. Cyster, and E.G. Engleman. 2002. Langerhans cells renew in the skin throughout life under steady-state conditions. *Nat. Immunol.* 3:1135–1141. doi:10.1038/ni852

Merad, M., F. Ginhoux, and M. Collin. 2008. Origin, homeostasis and function of Langerhans cells and other langerin-expressing dendritic cells. *Nat. Rev. Immunol.* 8:935–947. doi:10.1038/nri2455

Mildner, A., H. Schmidt, M. Nitsche, D. Merkler, U.K. Hanisch, M. Mack, M. Heikenwalder, W. Brück, J. Priller, and M. Prinz. 2007. Microglia in the adult brain arise from Ly-6ChiCCR2+ monocytes only under defined host conditions. *Nat. Neurosci.* 10:1544–1553. doi:10.1038/nn2015

Mohamadzadeh, M., F. Berard, G. Essert, C. Chalouni, B. Pulendran, J. Davoust, G. Bridges, A.K. Palucka, and J. Banchereau. 2001. Interleukin 15 skews monocyte differentiation into dendritic cells with features of Langerhans cells. *J. Exp. Med.* 194:1013–1020. doi:10.1084/jem.194.7.1013

Poulin, L.F., S. Henri, B. de Bovis, E. Devilard, A. Kissenpfennig, and B. Malissen. 2007. The dermis contains langerin+ dendritic cells that develop and function independently of epidermal Langerhans cells. *J. Exp. Med.* 204:3119–3131. doi:10.1084/jem.20071724

Stoitzner, P., L.K. Green, J.Y. Jung, K.M. Price, C.H. Tripp, B. Malissen, A. Kissenpfennig, I.F. Hermans, and F. Ronchese. 2008. Tumor immunotherapy by epicutaneous immunization requires langerhans cells. *J. Immunol.* 180:1991–1998.

Strid, J., S.J. Roberts, R.B. Filler, J.M. Lewis, B.Y. Kwong, W. Schpero, D.H. Kaplan, A.C. Hayday, and M. Girardi. 2008. Acute upregulation of an NKG2D ligand promotes rapid reorganization of a local immune compartment with pleiotropic effects on carcinogenesis. *Nat. Immunol.* 9:146–154. doi:10.1038/ni1556

Tripp, C.H., S. Chang-Rodriguez, P. Stoitzner, S. Holzmann, H. Stössel, P. Douillard, S. Saeland, F. Koch, A. Elbe-Bürger, and N. Romani. 2004. Ontogeny of Langerin/CD207 expression in the epidermis of mice. *J. Invest. Dermatol.* 122:670–672. doi:10.1111/j.0022-202X.2004.22337.x

Vesely, D.L., D. Fish, M.J. Shlomchik, D.H. Kaplan, and L.K. Bockenstedt. 2009. Langerhans cell deficiency impairs *Ixodes scapularis* suppression of Th1 responses in mice. *Infect. Immun.* 77:1881–1887. doi:10.1128/IAI.00030-09

Waskow, C., K. Liu, G. Darrasse-Jèze, P. Guermonprez, F. Ginhoux, M. Merad, T. Shengelia, K. Yao, and M. Nussenzweig. 2008. The receptor tyrosine kinase Flt3 is required for dendritic cell development in peripheral lymphoid tissues. *Nat. Immunol.* 9:676–683. doi:10.1038/ni.1615

Wolber, F.M., E. Leonard, S. Michael, C.M. Orschell-Traycoff, M.C. Yoder, and E.F. Srour. 2002. Roles of spleen and liver in development of the murine hematopoietic system. *Exp. Hematol.* 30:1010–1019. doi:10.1016/S0301-472X(02)00881-0

Langerhans cell proliferation | Chorro et al.